Predictive Control of Achilles Tendon Force During Cyclic Motions in a Simulated Musculoskeletal System With Parallel Actuation

Mahdi Nabipour, Gregory S. Sawicki, *Member, IEEE*, and Massimo Sartori, *Member, IEEE*

***Abstract*—Recent advancements in wearable exoskeletons for human lower extremities have primarily focused on augmenting walking capacity by either reducing metabolic costs or providing joint torque support based on measured electromyography or predicted joint torques. However, less attention has been given to the use of robotic exoskeletons for controlling the mechanics of specific biological tissues, such as elastic tendons. Achieving closed-loop control over in-vivo musculotendon mechanics during movement could revolutionize injury prevention and personalized rehabilitation. Here, we introduce a framework utilizing musculoskeletal modeling and nonlinear model predictive control (NMPC) to close the loop around tendon force in a simulation of cyclic force production of the human ankle plantarflexors in parallel with a powered exoskeleton. The proposed framework integrates a computationally efficient model comprising explicit closed-form ordinary differential equations governing musculotendon and ankle joint with parallel actuation dynamics. The model's computational time, in the microsecond range, allows prediction of future states in real-time closed-loop control. Compared to a predictive proportional-derivative controller, the NMPC-based framework more effectively maintained Achilles tendon force within a predetermined threshold across varying levels of muscle excitation amplitude and frequency. Remarkably, the NMPC framework demonstrates robustness to muscle excitation variations during cyclic motions, making it suitable for real-world applications.**

***Index Terms*—Locomotion, walking, hopping, ankle plantarflexors, Achilles tendon, musculotendon unit, hill-type muscle, predictive force control, injury prevention, wearable robotics.**

Received 14 June 2024; revised 30 November 2024 and 10 February 2025; accepted 21 March 2025. Date of publication 14 April 2025; date of current version 13 May 2025. This article was recommended for publication by Associate Editor S. Zhibin and Editor P. Dario upon evaluation of the reviewers' comments. This work was supported in part by the ERC Consolidator Grant ROBOREACTOR under Grant 101123866; in part by the ERC Proof of Concept Grant SMARTSENS under Grant 101113279; and in part by the Horizon 2024 RIA Grant SWAG under Grant 101120408. *(Corresponding author: Mahdi Nabipour.)*

Mahdi Nabipour and Massimo Sartori are with the Neuromuscular Robotics Laboratory, Department of Biomechanical Engineering, University of Twente, 7522 NB Enschede, The Netherlands (e-mail: m.nabipour@utwente.nl; m.sartori@utwente.nl)

Gregory S. Sawicki is with the Human Physiology of Wearable Robotics Laboratory, the George W. Woodruff School of Mechanical Engineering, the School of Biological Sciences, and the Institute for Robotics and Intelligent Machines, Georgia Institute of Technology, Atlanta, GA 30332 USA (e-mail: gregory.sawicki@me.gatech.edu).

This article has supplementary downloadable material available at https://doi.org/10.1109/TMRB.2025.3560385, provided by the authors.

Digital Object Identifier 10.1109/TMRB.2025.3560385

I. Introduction

DEVELOPING wearable exosuits and exoskeleton technologies capable of providing closed-loop control over musculotendon forces, especially during dynamic activities such as walking and hopping, represent an open challenge. Addressing this challenge has great potential to enable high-precision assistive robots that can specifically support targeted tissues, such as biological tendons. This would enable robotic systems to control mechanical strains in a closed-loop manner, reducing the risk of biological tissue injuries caused by repetitive or high-impact activities. Additionally, such systems could enhance the rehabilitation of targeted tissues and support healthy aging. Currently, there are no robotic exoskeletons capable of controlling in closed-loop the mechanical loads acting on biological tendons across various locomotion tasks, e.g., there is no robot that can ensure tendon forces never exceed predefined upper boundaries, regardless of the mechanical demand of the motor tasks such as external locomotion speed, frequency, and loads.

Researchers have previously employed a range of control techniques based on heuristics [1], optimization for energy expenditure using human in the loop (HIL) [2], [3], [4], chemical energy used by the muscle [5], walking speed [6], or user preference [7]. Moreover, controllers have been designed using real-time estimations of an individual's joint moment to offer support profiles that correspond with the subject's tailored musculoskeletal mechanics. These approaches encompass proportional myoelectric control [8], real-time EMG-driven model-based techniques [9], and deep neural network-based proportionate joint moment control [10]. Notably, these controllers operated at the joint moment level rather than within the biological tissue level.

The researchers employed a force-controlled robotic device to apply tissue stresses on mice, assessing the impact of mechanical loads on muscle repair post-injury [11]. A few studies enabled proportional assistance based on measured Achilles tendon force profiles. In a recent study, the Achilles tendon force was controlled using nine predefined plantarflexion assistance profiles [12]. Nuckols et al. developed an ankle torque profile for the wearer by utilizing ultrasound measurements of soleus velocity during walking with the aim of reducing metabolic cost. These measurements were analyzed offline afterwards, in approximately 5 seconds to process images and generate torque profiles. This processing time is significantly less than the fastest HIL investigated by

Slade et al. [13]. However, none of these studies explored the possibility of closed-loop control of musculotendon loads, such as Achilles tendon force.

Current state-of-the-art lower limb exoskeleton controllers lack direct closed-loop control over biological tissue parameters, such as musculotendon unit (MTU) peak force. Our research aims to fill this gap by developing a predictive-based control framework that can steer tissue loading in a targeted, assist-as-needed (AAN) manner, specifically to control peak Achilles tendon force during cyclic motion. This requires 1) the ability to predict how biological loads will vary in the future in response to device assistance, and 2) a predictive controller that discovers the optimal assistive torque needed to influence the tendon force future trajectory. Here, we developed a nonlinear model predictive control (NMPC) approach that leverages the integrated human-exoskeleton system as the core model and employs direct collocation to solve the optimal control problem. This NMPC controller operates by receiving feedback from the simulated musculoskeletal system's states and then optimizing the assistive profile based on future predictions of tendon force. While NMPC has previously been employed to generate optimal joint trajectories [14] and assistive device joint torques [15], its application to controlling musculotendon mechanics represents a novel endeavor. This innovative approach shows potential for achieving precise control over peak tendon force, enabling the development of computationally efficient AAN control strategies.

The model-based controllers such as NMPC require a model of the MTU system. Widely adopted for modeling MTU dynamics are Hill-type models, chosen for their efficiency and fewer parameters compared to alternatives like Huxley's model of muscle contraction [16], [17]. The literature presents several mathematical formulations that model Hill-type muscle contraction and tendon strain mechanics. These formulations utilize nonlinear splines to interpolate experimentally derived data, capturing muscle force-length-velocity and tendon force-strain relationships. However, existing formulations often rely on conditional statements [18], [19], not leading to closed-form equations. This reliance on conditional statements poses challenges when integrating these formulations into control theory frameworks and MPC schemes. The inner model of NMPC ideally requires a closed-form equation, ensuring computational efficiency for online implementation.

Limited research has focused on deriving closed-form equations for muscle contraction dynamics. Previous studies have provided closed-form ordinary differential equations (ODEs) for various conventional Hill-type muscle models [20]. While van den Bogert et al. [21] introduced an implicit formulation for the Hill-type muscle model, it was not in ODE form. Building on this groundwork, De Groote et al. proposed both computationally efficient implicit and explicit formulations for estimating muscle forces during motion using direct collocation optimal control [22]. In the context of MPC schemes, it is crucial for the formulation to be in a differential form to facilitate future predictions through time integration, a feature currently absent in the literature. The ODE formulations of the existing conventional Hill-type muscle model [20] encounter difficulties at low muscle activations due to the lack of inherent damping in the Hill model, thereby restricting their applicability in predictive control scenarios [22], [23]. In a previous investigation, uni-variate linear regression was utilized to derive a closed-form solution for the damped Hill-type muscle model [24], [25]. However, the derived model lacked generalizability across different gaits and muscle groups.

This paper presents three novel contributions:

- It introduces a closed-form ODE formulation for the Hill-type muscle model, incorporating parallel damping.
- A state-space representation of a combined human and exoskeleton model is proposed for MTU force control.
- Furthermore, a predictive framework is developed for controlling MTU forces.

We first present an explicit, closed-form, and differentiable set of equations for: 1) damped Hill-type muscle contraction dynamics by linearizing the muscle force-velocity (F-V) curve, and 2) motion dynamics of a simplified multi-body dynamic system of the human leg actuated by a lumped model of the triceps surae MTUs with a parallel artificial actuator (mimicking the assistance of an ankle exoskeleton). These components are integrated into an NMPC framework for the predictive and adaptive control of peak tendon force during cyclic motions with a focus on hopping in this research. To address computational time concerns of implicit methods and divergence issues with explicit formulations, we propose an approach utilizing the linearization of the damping-incorporated Hill-type muscle model, as employed in our previously developed Calibrated EMG-Informed Neuromusculoskeletal Modelling (CEINMS) toolbox [26], [27], to enhance stability, accuracy, and generalizability of the closed-form contraction dynamics. The resulting model is augmented with a human leg model actuated by lumped MTUs and transformed into state-space form, ideal for designing various controllers. This combined model serves as the inner model for an NMPC algorithm, effectively controlling Achilles tendon force during cyclic simulations. This framework is applicable to controlling MTU forces in the lower limbs during walking at various speeds [28], [29], hopping with different frequencies, and can be extended to address MTU forces in the trunk/upper limb [30].

II. Methods

In this section, we provide the modeling and control of the human-exoskeleton system in detail. We begin by describing the modeling methodology that was developed in order to create the closed-form model of the damped Hill-type muscle. Next, we describe how this MTU model can be integrated with a model of cyclic motion (e.g., hopping) and parallel exoskeleton assistance for controlling the musculotendon force.

A. Modeling the MTU Dynamics

We employ a Hill-type model with pennation angle to describe the dynamics of musculotendon contraction [18], [31]. The conventional form of this model consists of a contractile element in a combination of series and parallel arrangements with elastic elements. When addressing the presence of compliant tendons in Hill-type models, the governing ODE takes the following form:

$$\dot{F}^T = k^T\left(\dot{L}^{MT} - \dot{L}^M\cos(\alpha) + L^M\dot{\alpha}\sin\alpha\right) \tag{1}$$

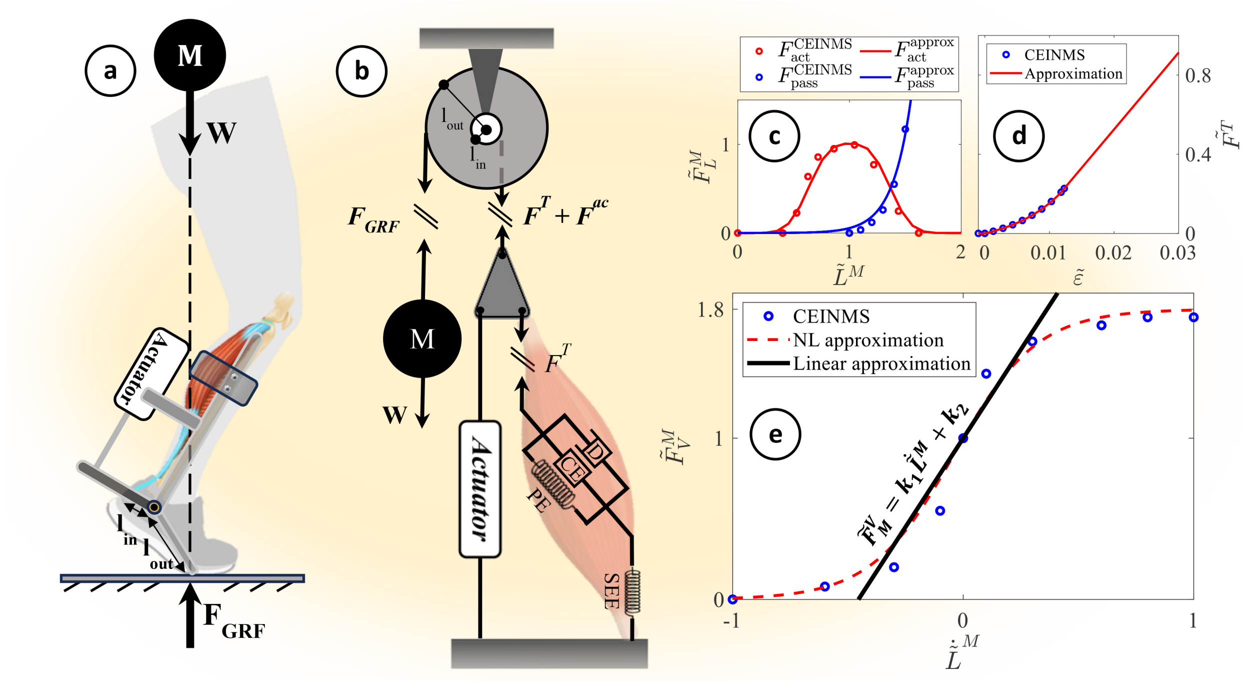

Fig. 1. Human-exoskeleton system in **(a)** experimental setup and **(b)** simulation environment. (c-e) Functions used for muscle-tendon force generation: **(c)** Active and passive muscle force-length relationships, **(d)** tendon force-strain relationship, and **(e)** muscle force-velocity relationship. CEINMS model outputs (dots) are approximated using nonlinear (NL) and linearized functions (dashed and solid lines).

where α denotes the pennation angle of the muscle. F^T represents the tendon force, k^T the tendon stiffness, L^M the muscle fiber length, and L^{MT} the MTU length. The MTU parameters—specifically, the optimal fiber length and tendon slack length—are determined as weighted averages across the triceps surae muscles and extracted from CEINMS. In CEINMS, the active and passive force-length (F-L) and F-V parameters are modeled as cubic B-splines [19]. We employ the equations outlined in [20] to describe the active and passive F-L elements within the MTU contraction dynamics (Figure 1-c).

The series elastic element of the muscle fiber (SEE) is mostly represented as stiffness, offering resistance to stretching. In CEINMS, the stiffness is derived as a mean from diversely collected data, exhibiting a nonlinear relationship with strain. To capture this nonlinear behavior, two approaches were possible: a) approximate the tendon force-strain data with regression, Figure 1-d), or b) approximated the stiffness, modeled as splines in CEINMS, using a high-order polynomial function, as used in [24].

1) Damped Hill-Type Muscle Model: The MTU length and the pennation angle are directly determined through limb kinematics [19]. However, muscle fiber length is computed by integrating the inverse of the muscle's F-V relation. Although there is a closed-form solution for the ODE of this type of Hill-type muscle model [20], but the model is unstable whenever the activation approaches near zero. To tackle this challenge, some proposed models integrate parallel damping within the muscle fiber [23], [26], illustrated in Figure 1. The governing equation of the damped Hill-type model is derived as:

$$\frac{F^T}{\cos(\alpha)} = F_O^M\left(a(t)\tilde{F}_L^M\tilde{F}_V^M + \tilde{F}^{PE} + \tilde{F}^D\right). \tag{2}$$

Here, F_O^M, $\tilde{F}_L^M$, $\tilde{F}^{PE}$, and $\tilde{F}_V^M$ denote the maximum isometric force, normalized active and passive force-length, and the normalized F-V relation of the muscle. Also, $a(t)$ signifies muscle activation, calculated through first-order activation dynamics [31], and $\tilde{F}^D$ represents the normalized viscous damping determined as:

$$\tilde{F}^D = b.\dot{\tilde{L}}^M \tag{3}$$

where the variable b represents the damping coefficient for the damped hill-type muscle.

2) Linearizing F-V Relation: When considering the damped Hill-type muscle model, deriving an analytical closed-form solution is not feasible. To address this challenge and obtain a closed-form solution for (1), we can leverage the observation that during activities such as walking and running, the normalized velocity of lower limb eccentric and concentric contractions typically stays within the range of ± 0.5 [23]. This simplification facilitates the streamlining of the F-V relationship, making it possible to derive a closed-form solution for the damped Hill-type muscle model. As indicated in Figure 1, the F-V relationship employed in the CEINMS toolbox appears almost linear within the normalized velocity range of ± 0.5. Consequently, we can approximate the muscle's nearly exponential behavior as linear in this specific velocity range. Using this assumption we obtain:

$$\frac{F^T}{\cos(\alpha)} = F_O^M.\left(a(t).\tilde{F}_L^M(k_1\dot{\tilde{L}}^M + k_2) + \tilde{F}^{PE} + b.\dot{\tilde{L}}^M\right) \tag{4}$$

where k_1 and k_2 represent the parameters of the linear approximation of the F-V relation within the range of ± 0.5. These values can be determined through regression, either by considering the entire active range of the muscle, the range between ± 0.5, or the specific region where we have prior knowledge that the muscle will be active based on the given task. In our simulations we assumed $k_1 = 2.2$ and $k_2 = 1$ which best matches the approximate nonlinear normalized F-V relation for $\dot{L}^M$ in the range of ± 0.4. Using these assumptions, the only unknown parameter of equation (1), $\dot{L}^M$, can be obtained:

$$\dot{L}^M = V^{max}\left(\frac{\frac{F^T}{\cos(\alpha)} - F^{PE} - k_2 a F_O^M \tilde{F}_L^M}{F_O^M\left(k_1 a \tilde{F}_L^M + b\right)}\right) \tag{5}$$

B. NMPC Design for Tendon Force Control

The predictive controller framework comprises three major components: a) tendon force predictor, b) desired force estimator, c) NMPC algorithm. a combined model of the MTU and a motion-related ODE is used as the inner model of the NMPC and within the tendon force predictor.

1) Models Used for Control: In this paper, we investigated how the coupled system of a human-exoskeleton device responded to varying frequencies and magnitudes of muscle excitation during a rhythmic movement (i.e., human hopping). This motion heavily depends on the ankle MTUs, particularly the triceps surae Achilles tendon complex, accounting for a substantial portion (up to 80%) of the limb's total positive mechanical power to meet the mechanical work requirements of the task. The closed-form ODE obtained for the tendon force estimation, should be extended with another equation that relates the tendon force to the movement. For example, Robertson et al. [32], [33] proposed a simplified model of the human leg to capture the salient features of rhythmic locomotion. In their proposed model, they used a non-pennated Hill-type muscle without parallel damping to represent the triceps surae. This model is verified and valid for the cases that the subject does not undergo deep knee bends. By introducing a parallel actuator to this model, a combined exoskeleton-MTU model is obtained (Figures 1-c and 1-d). The governing equations for this model are as follows:

$$\dot{F}^T = k^T\left(\dot{L}^{MT} - \dot{L}^M\cos(\alpha) + L^M\sin(\alpha)\dot{\alpha}\right) \tag{6a}$$

$$\ddot{L}^{MT} = -\frac{g}{W}\left(\frac{l_{in}}{l_{out}}\right)^2\left(F^T + F^{ac} - W\frac{l_{out}}{l_{in}}\right) \tag{6b}$$

where $\ddot{L}^{MT}$ is the linear acceleration of the lumped MTU. In this equation, the ratio l_{in}/l_{out} represent the inverse of the mechanical advantage of the pulley-mass system shown in Figure 1-b. Also, W and g are the portion of the body weight carried by each leg's lumped MTU and the gravitational acceleration, respectively. The assistive actuator force, F^{ac}, is provided by the exoskeleton. The coupled equations above can be expressed in the state-space form:

$$\dot{x} = f(x, u, a(t)), x = \left[F^T\ L^{MT}\ \dot{L}^{MT}\right]^{\mathbf{T}}, u = F^{ac} \tag{7}$$

where the symbol $\mathbf{T}$ denotes the transpose operation. Since the final equation is in state-space form, the derived combined model is suitable for designing different linear and nonlinear model-based controllers.

To derive the combined model of the human leg and the wearable parallel assistive device, the mass was represented as half of the body mass (35 kg) to approximate the loads experienced by each leg [33]. Moreover, the model incorporated a maximum isometric force of 4000 N, which was derived from the summation of the maximum isometric force of the triceps surae muscle group. It also employed first-order activation dynamics with activation and deactivation time constants of 0.091 and 0.015 seconds, respectively.

2) Optimization: The aim of the NMPC algorithm is to minimize the following cost function while keeping the tendon force under a predefined threshold:

$$J = \sum_{k=1}^{\mathrm{N}} w_1\left(F^{ac}\right)^2 + w_2\left(\Delta F^{ac}\right)^2 + w_3\left(F_k^T - F_{des}^T\right)^2 \tag{8}$$

where w_i weight the contribution of tendon force, the actuator force (F^{ac}), and its increment (ΔF^{ac}) on the value of the cost function. This cost function is minimized over the entire control horizon.

In this work, we assume that the muscle activation is preknown, which is considered valid, particularly in the context of employing muscle synergies for cyclic motions. As a result, we utilize this predetermined activation as input for both the MTU model and the forward dynamics human motion model integrated into the tendon force predictor and the inner model of the control framework. Additionally, the interior-point method is employed as the solver for conducting the direct collocation optimization, with the dynamics enforced as an equality constraint.

The initial control horizon is set to 150 ms, within which the tendon force predictor (Figure 2) predicts the future tendon force at time t (Figure 3). After estimating the predicted tendon force, should the system detect a maximum value of the tendon force surpassing the threshold (one of NMPC's constraints), it identifies the corresponding time of occurrence. If the time of occurrence is less than 150 ms, it is designated as the new control horizon, provided it is not lower than a preselected minimum horizon of 100 ms [34]. For computational cost purposes, similar to the zero-older hold (ZOH) method, the controller output is computed every few steps. Therefore, the control horizon determined within the given time frame is subsequently divided by the value of the ZOH and rounded the nearest integer less than or equal to that element.

$$\text{Horizon (steps)} = \left\lfloor \frac{\text{Horizon (ms)}}{\text{ZOH (ms)}} \right\rfloor \tag{9}$$

In the event that the maximum predicted tendon force exceeds the tendon force threshold, the controller is triggered, and consequently, an estimated desired tendon force value must be determined for the controller to track. Two strategies are possible for deriving the desired tendon force. One method involves setting the desired value equal to the threshold whenever the predicted value surpasses the threshold, and equal to the predicted value when it remains below the threshold. Another approach, which exhibited greater robustness in simulations, entails defining the desired tendon force such that when the threshold is crossed during tendon force prediction,

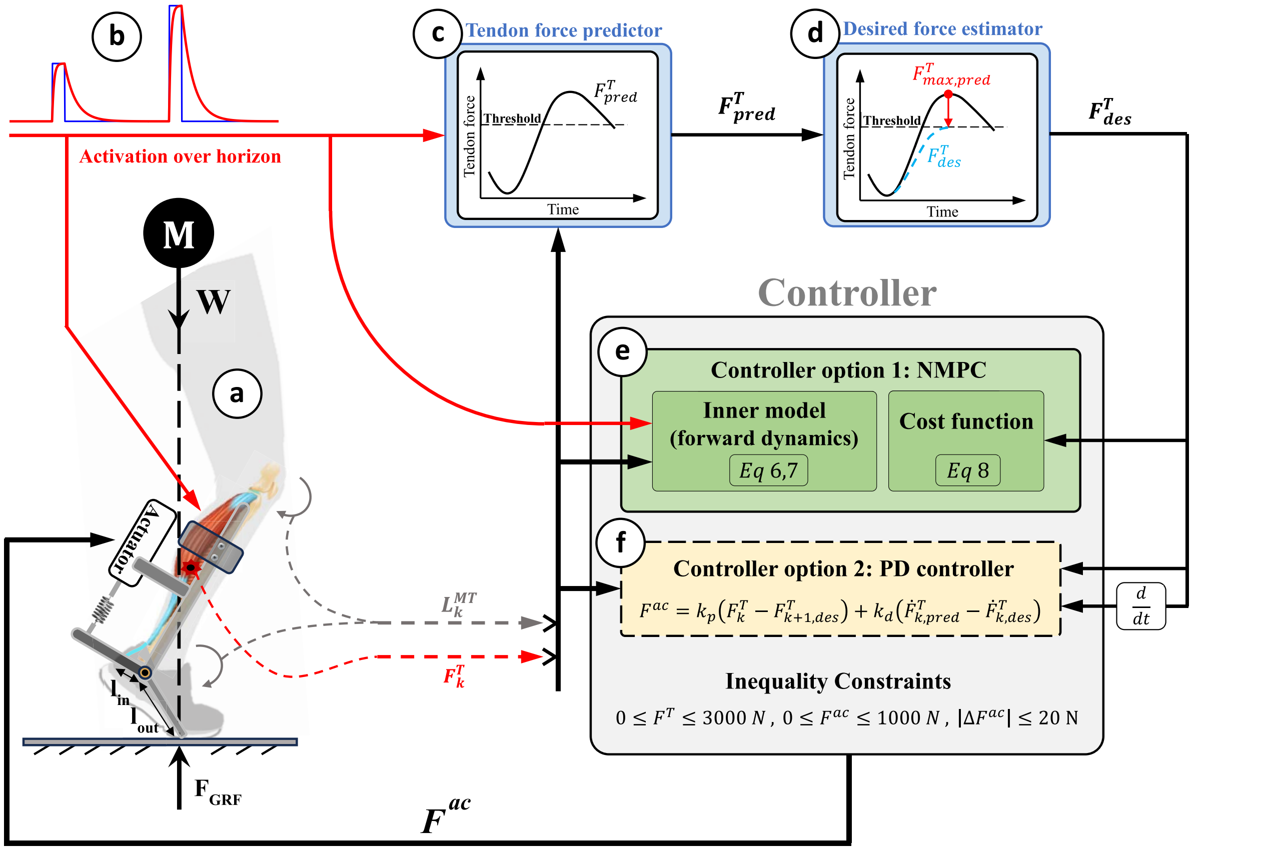

Fig. 2. Illustration of the predictive control framework for a human-exoskeleton system. **(a)** A closed-form model in state-space form emulates the coupled dynamics. In practice, MTU length (L^{MT}) and muscle activation are estimated from the joint angles and the EMGs, respectively, using online NMS models (e.g., CEINMS). **(b)** In simulations, L^{MT} is derived from model dynamics (6b), and activation is either known or predicted via synergies. **(c)** Future MTU force is predicted using forward dynamics ((6a) and (6b)) based on muscle activation over the horizon. **(d)** If tendon force exceeds the threshold, a desired force is generated, capped at this threshold (Fig. 3). **(e)** For NMPC, current L^{MT} and predicted activation are input into the inner model, with desired tendon force incorporated into the cost function. **(f)** For predictive PD control, the next step of the desired MTU force and its derivative are supplied, and the controller output updates the coupled system dynamics.

the maximum desired tendon force is set to match the threshold value at the same instance the maximum tendon force is predicted to happen. Subsequently, the remaining values before the maximum are linearly scaled down to construct the complete desired tendon force profile as:

$$\boldsymbol{F}^{T}_{pred,des} = F^{T}_{k} + \frac{F^{T}_{thresh} - F^{T}_{k}}{F^{T}_{max} - F^{T}_{k}} \left(\boldsymbol{F}^{T}_{fut} - F^{T}_{k} \right) \tag{10}$$

where F^{T}_{thresh} represents the tendon force threshold, F^{T}_{max} is the maximum predicted tendon force over the control horizon, and $\boldsymbol{F}^{T}_{fut}$ is the predicted tendon force over the control horizon. Note that the bold parameters in the equation are vectors. The values following the occurrence of the maximum are set to be equal to the threshold value (Figure 3).

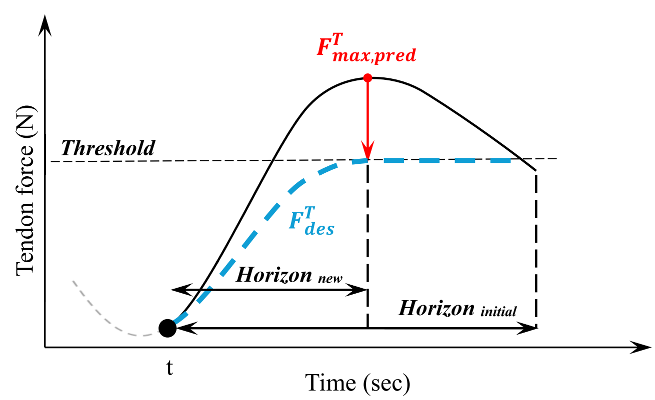

Fig. 3. Estimation of the desired future MTU force based on the predicted MTU force within the predictive framework.

C. Validation Procedures

To evaluate the effectiveness of the control structure, the performance of the NMPC approach was compared with both constrained and non-constrained predictive PD algorithms. Following this comparison, a sensitivity analysis of the NMPC approach was conducted.

1) Control Approach: In the initial set of simulations, the performance of the NMPC controller was benchmarked against that of a predictive PD controller. For this comparison, the NMPC component (Figure 2-e) within the control structure was substituted with a PD controller (Figure 2-f). This PD controller was defined by gains of $K_p = 0.5$ and $K_d = 0.05$, which were fine-tuned through trial and error. The aim was to consistently maintain the tendon force below the threshold while also ensuring it remained in close proximity to the threshold value. The predictive PD controller was once operating without and once subjected to the same constraints as the NMPC. For both NMPC and predictive PD, the controllers' objective is to keep the Achilles tendon force under 3000 N. Also, the sensitivity of the NMPC controller was investigated with respect to variations in activation and the subject's weight.

2) Sensitivity Analysis: In order to examine the sensitivity of the controller to the muscle excitation, the muscle excitation that is used in the control framework (in the tendon force predictor and NMPC inner model) is perturbed according to:

$$\epsilon^{cont}_{k=1,\ldots,hor} = \left(1 + d^{\epsilon}\right)\epsilon_{k=1,\ldots,hor} \tag{11}$$

where d^{ϵ} is the disturbances value which is the muscle excitation supplied to the human-exoskeleton combined model. $\epsilon_{k=1,\ldots,hor}$ represent the muscle excitation supplied to the human-exoskeleton combined model (green and red dotted lines in Figure 7-b, and $\epsilon^{cont}_{k=1,\ldots,hor}$ is the muscle excitation supplied into the tendon force predictor and NMPC controller's inner model (black dotted line in Figure 7-b). This excitation is then converted into muscle activation (solid lines in Figure 7-b) using first-order activation dynamics.

The controller's estimation of the subject's weight can be affected by two primary scenarios: a) when the subject alters their weight, for example, by adding or removing load from a backpack; and b) unforeseen variations in the center of pressure (CoP). Although CoP typically concentrates around the metatarsophalangeal joints during hopping (also true for late-stance walking), a specific optimal point for the CoP can be identified for estimating l_{out} in Figure 1. It's worth noting that in practical scenarios of hopping and walking, slight variations in the CoP position may occur. These variations in CoP can impact the l_{out}/l_{min} ratio, consequently affecting the load carried by the parallel lumped muscle-exoskeleton complex model. Therefore, the maximum tendon force in each period of hopping can be evaluated by changing the felt load on the muscle according to:

$$W_{hum} = \left(1 + d^{w}\right)W_{cont} \tag{12}$$

where W_{hum} and W_{cont} are the weights that are supplied into the human-exoskeleton combined model and the controller, respectively and d^{w} represents the disturbance value. in this case, the controller isn't aware of the change made in the weight of the subject but the subject undergoes the different weights in the model.

To further validate the framework's robustness, we conducted complementary work (detailed in [35]) examining how the choice of linearized F-V slope impacts controller performance when applied to different muscle fiber types, with fast- and slow-twitch specific adaptations."

III. Results

A. Modeling and Validation

Simulating the muscle contraction dynamics using the data collected during plantarflexion and dorsiflexion on the dynamometer [36], shows that the model presented in [24] becomes unstable whenever the activation is close to zero.

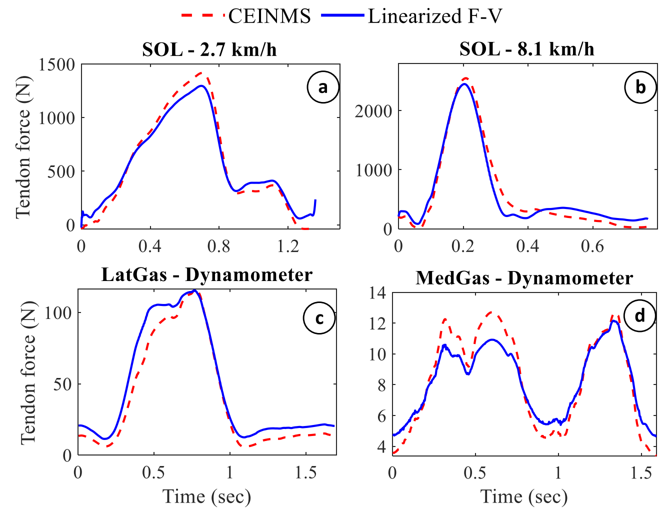

Fig. 4. Comparison of tendon force predictions using the CEINMS model (dashed red) and a Hill-type muscle model with parallel damping and a linearized force-velocity (F-V) relationship (solid blue). Panels **(a)** and **(b)** show the soleus (SOL) muscle under walking (2.7 km/h) and running (8.1 km/h) conditions, respectively [37]. Panels **(c)** and **(d)** present the lateral (LatGas) and medial (MedGas) gastrocnemius muscles during dorsiflexion and plantarflexion on a dynamometer [36].

To evaluate the precision of the MTU modeling method, the estimated MTU force of the model for the plantarflexor muscles has been examined over a wide range of movement speeds and frequencies, including walking and running [37], along with dorsiflexion and plantarflexion on a dynamometer [36]. To prevent redundancy, a representative condition for each task has been illustrated: 2.7 km/h for walking involving the Soleus muscle, 8.1 km/h for running involving the Soleus muscle, and the muscle forces of the Medial Gastrocnemius and Lateral Gastrocnemius while the subject followed sinusoidal position targets with an amplitude of 0.15 rad at 0.6 Hz on the dynamometer are presented in Figure 4. The normalized root mean square error (NRMSE) and the correlation coefficient (R^2) between the linearized model and the values estimated by the CEINMS toolbox for dorsiflexion/plantarflexion data of the lateral and medial Gastrocnemius are computed as 7.7% (with $R^2 = 0.966$) and 5.2% ($R^2 = 0.937$), respectively. Additionally, for gait data collected at different speeds, the NRMSE values are 5.2% (with $R^2 = 0.982$) for walking at 2.7 km/h and 5.7% (with $R^2 = 0.98$) for running at 8.1 km/h. Note that the plots for the lateral and medial Gastrocnemius represent averages over multiple periods of sinusoidal movement.

B. Control

The investigation into the computational time required for the NMPC involved testing various ZOH values. It was found that a system with 16 GB of RAM and an Intel Core i7-11800H @ 2.30GHz processor could complete each optimization iteration in MATLAB software within 14 ms when using a ZOH of 10. The interior-point optimizer was set to a maximum of two iterations to reach the optimal solution. This timeframe falls within the range of the physiological electromechanical delay [38].

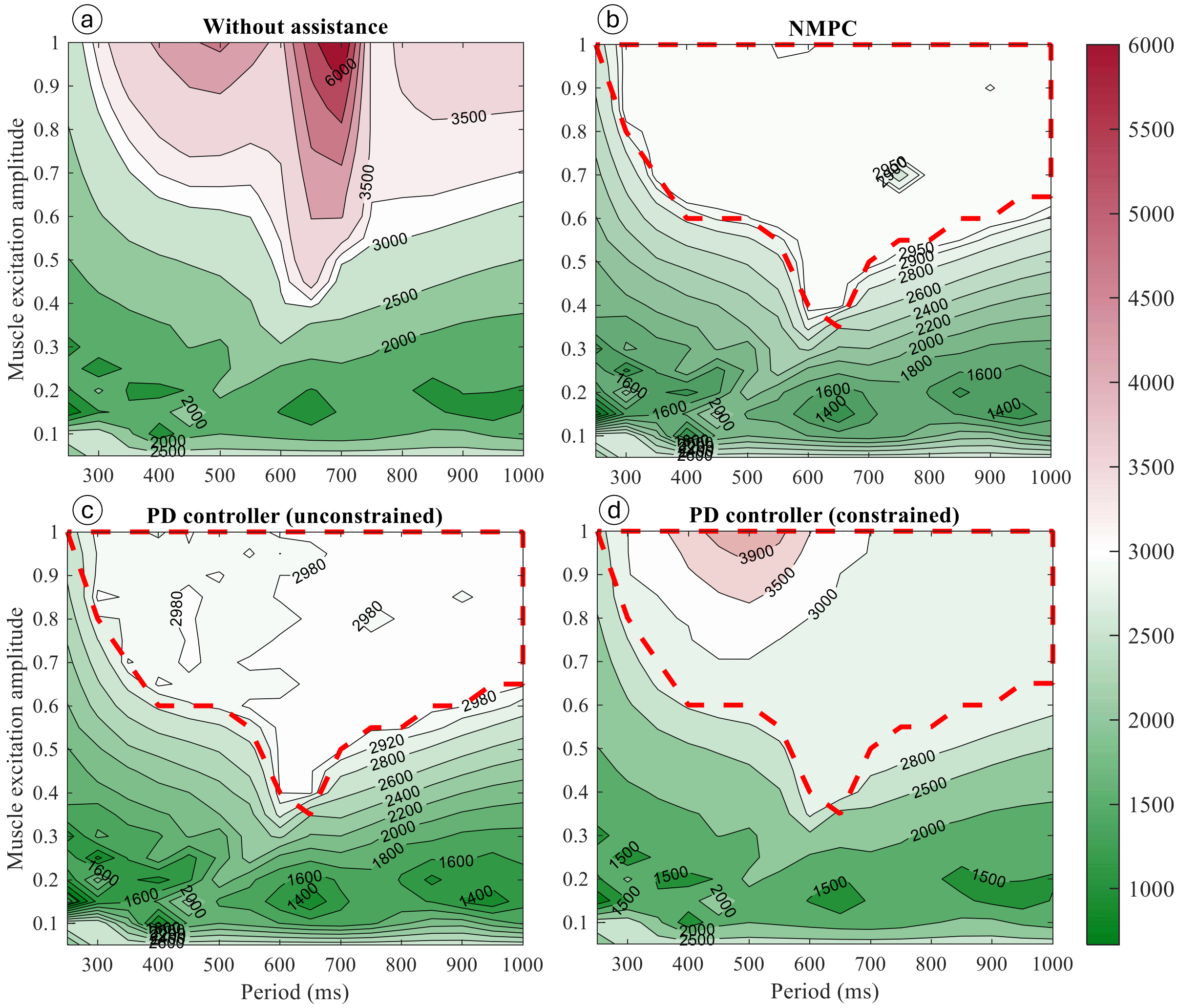

Fig. 5. The peak MTU force values (in Newtons) **(a)** without assistance as a function of muscle excitation period (x-axis) and amplitude (y-axis). The values of the contours represent the maximum tendon forces (in N) for each muscle excitation period and amplitude. Performance of **(b)** NMPC, **(c)** non-constrained, and **(d)** constrained predictive PD in maintaining the peak MTU force below the threshold of 3000 N. The red dashed lines indicate instances where the tendon force predictor recognizes a surpassing of the threshold within the control horizon, thereby activating the controller.

For the purpose of comparing both NMPC and predictive PD, the muscle undergoes excitations ranging from 0.05 to 1 with increments of 0.05. Additionally, the period experiences various values, ranging from 250 ms (corresponding to a frequency of 4 Hz) to 1000 ms (corresponding to a frequency of 1 Hz), with increments of 50 ms.

Figure 5 illustrates the effectiveness of both NMPC and (non)constrained predictive PD in maintaining the tendon force below the predefined 3000 N threshold. The contour plots depict the maximum tendon force values at each period and amplitude of muscle excitation. In these plots, the x-axis represents the period in milliseconds, and the y-axis represents the amplitudes of muscle excitation. When the user undergoes different excitation periods and amplitudes without receiving any assistance, the maximum tendon force is plotted in Figure 5-a. The parts of the figure which are in green, are the parts that the Achilles tendon force is maintained under 3000 .

The peak tendon force exceeds the threshold when no support is provided by the parallel assistive device, particularly during periods of high excitation amplitude. This trend is also observed in the assistive force generated by the constrained PD controller. In the case of NMPC, the maximum tendon force achieved is characterized by a peak value of almost 3002.4 N, a median of 2993.7 N, a standard deviation (STD) of 57.3 N, and a NRMSE of 2%. However, for the non-constrained predictive PD controller, these values shift slightly to 3001.8 N (maximum), 2989 N (median), 55.2 N (STD), and 2.1% (NRMSE). In the case of the constrained PD controller, these values were 4179 N (maximum), 2995.8 N (median), 258.6 N (STD), and 9.1% (NRMSE). These statistics are presented in Table I for clarity. The control profiles generated

TABLE I
MAXIMUM, MEDIAN, AND STD OF PEAK MTU FORCES IN EVERY HOP UNDER DIFFERENT CONTROLLERS

Controller	Max (N)	Median (N)	STD (N)
NMPC	3002.4	2993.7	57.3
Non-Constrained PD	3001.8	2989.0	55.2
Constrained PD	4179.0	2995.8	258.6

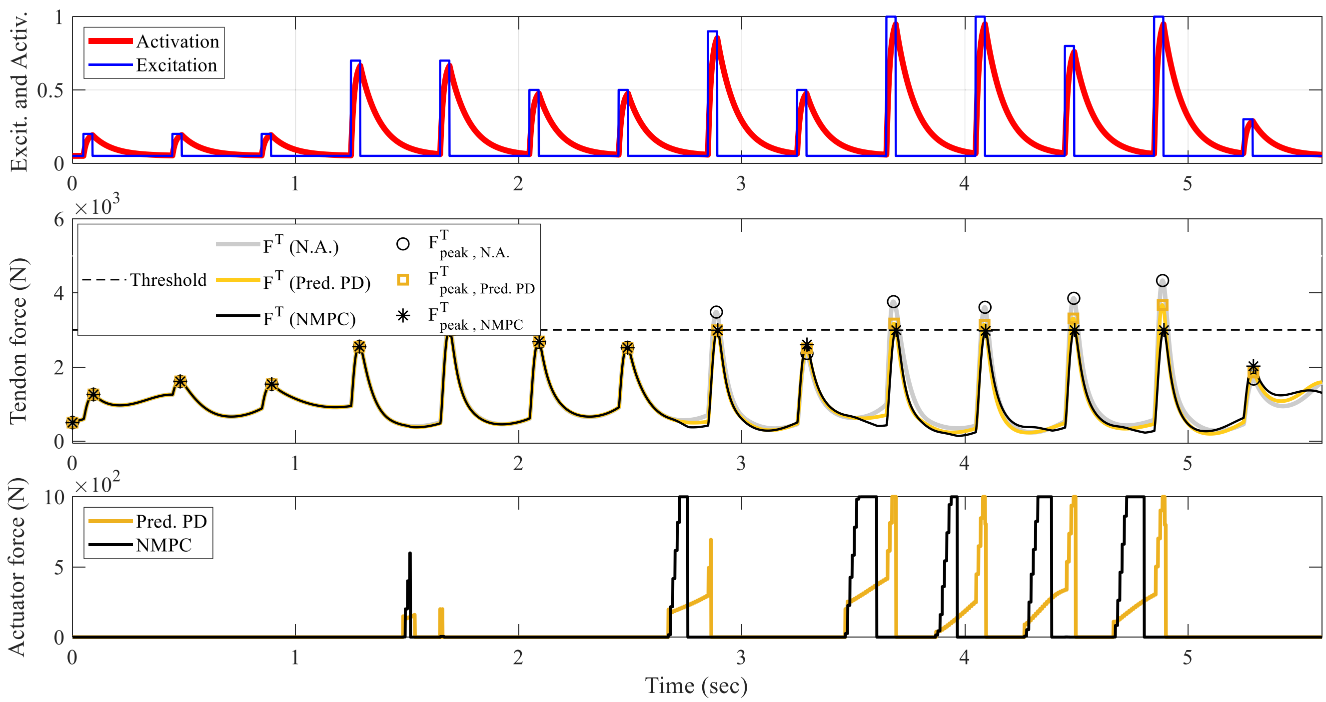

Fig. 6. Comparison of NMPC and Predictive PD control performance in controlling MTU force below 3000 N threshold. The visualizations from top to bottom include muscle excitation and activation for various excitation amplitudes during hopping with a period of 400 ms (2.5 Hz), MTU force with and without assistance, and exoskeleton actuation in both NMPC and Predictive PD control scenarios.

TABLE II
IMPACT OF MUSCLE EXCITATION AMPLITUDE UNCERTAINTY ON THE MEDIAN, STD, AND NRMSE OF PEAK MTU FORCES DURING EACH HOP UNDER NMPC CONTROL

Uncertainty (%)	Median (N)	STD (N)	NRMSE (%)
+10	2790	14.5	7.0
+20	2609	21.9	12.7
−10	3219	68.5	6.7
−20	3471	166.0	14.0

by both NMPC and constrained PD controllers under different activation levels are illustrated in Figure 6.

1) Sensitivity of NMPC to Muscle Excitation: To examine the sensitivity of the controller to activation, instead of inputting the actual future activation into the tendon force predictor (Figure 7-a) and the controller's inner model, a perturbed vector of the future activation (Figure 7-b) was utilized. The perturbation added to the muscle excitation is changed between -0.2 to $+0.2$ with the increment of 0.1. Figure 7-c shows the controller's performance in response to the different values of disturbance in the excitation.

When the uncertainty in the muscle excitation is $+10\%$, the maximum tendon force achieved is characterized by a median of 2790 N, STD of 14.5 N, and a NRMSE of 7% when compared with the 3000 N threshold. For $+20\%$ uncertainties, these values change into a median of 2609 N, STD of 21.9 N, and a NRMSE of 12.7%. Conversely, when the uncertainty decreases by -10% and -20%, the median/STD/NRMSE values increase to 3219/3471 N, 68.5/166 N, and 6.7/14%, respectively. All these statistics (Table II) correspond to the values at which the MTU force would have exceeded the threshold if assistance had not been provided.

2) Sensitivity of NMPC to the Weight: Figure 7-b illustrates the controller's performance under non-assisted and assisted conditions as the disturbance values vary from -40% to +40%. In the absence of assistance, the maximum MTU force reaches 4320N under the highest excitation level. With a 40% decrease in subject weight, the maximum MTU force without assistance decreases to 3616N. If the predictive control framework is unaware of this weight change, potentially due to a variation in the subject's backpack load, the controller limits the peak MTU force to 2345N, although the threshold should have remained at 3000N. The maximum MTU load with a 20% decrease in activation amplitude remains below 2722N. Also, with a 20% and 40% increase in subject weight, the maximum MTU force rises to 3163 N and 3247 N, respectively.

IV. DISCUSSIONS

We presented a framework for the predictive closed-loop control of peak Achilles tendon force during cyclic motions in a simulated musculoskeletal ankle joint system with parallel actuation. We introduced a closed-form formulation for the modified Hill-type muscle model and derived explicit closed-form equations for simulating cyclic motions of the combined human-exoskeleton system.

A. Modeling

In a previous study, we introduced a uni-variate linear regression method to find a curve function for estimating $\dot{L}^M$ instead of using equation (5) [24]. The method proposed for linearizing the force-velocity relation in this paper eliminates the necessity for individual muscle optimization, presenting a significant advantage over the regression technique.

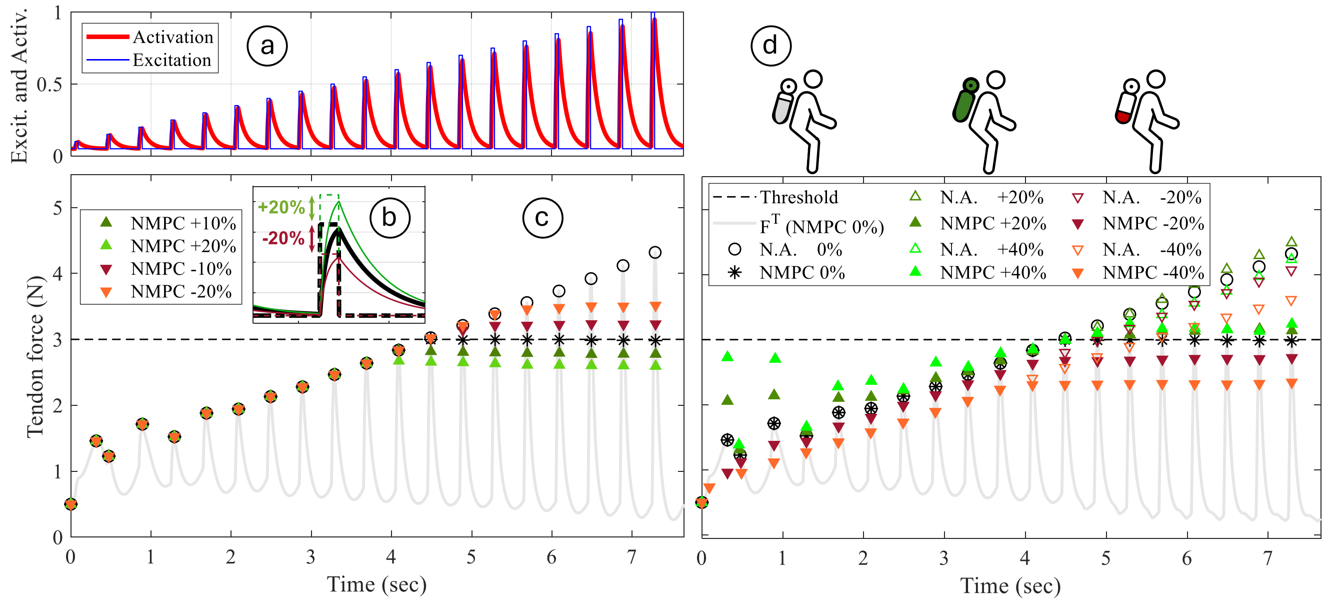

Fig. 7. Examination of the NMPC controller's sensitivity to variations in muscle excitation amplitudes and user weight, assuming a standard user weight of 70 kg (35 kg per leg) with consistent muscle excitation patterns. **(a)** Muscle excitation ranges from 0.05 to 1 in 0.05 increments. **(b)** Perturbations in muscle excitation are simulated, where the controller's perceived excitation (black dashed line) differs from actual excitation (green for higher, red for lower). **(c)** Sensitivity analysis shows peak forces with reduced excitation (red/orange triangles) or increased by 10% and 20% (light/dark green triangles). **(d)** Peak MTU forces under varying user weights are analyzed, e.g., "N.A. +40%" indicates no assistance with a 40% weight increase unknown to the controller.

Notably, results illustrated that the proposed model exhibited generalization capabilities across different muscle activation dynamics, while capturing the desired muscle-tendon behavior at various speeds and frequencies of representative cyclic motions (Figure 4). Moreover, the incorporation of damping in the Hill-type muscle model enhanced model stability, i.e., the muscle-tendon unit did not diverge as muscle activation approached zero. This stability contrasts with scenarios where damping is not utilized [25] or when employing the regression method [24].

As depicted in Figure 4, the model demonstrated accuracy (6.2% error in average) in estimating peak MTU forces when compared to reference profiles. Moreover, the computational costs associated with the full set of equations, comprising of muscle-tendon dynamics and the equation of motion for the human leg with parallel exoskeleton actuation, was substantially low, $3\mu s$ per iteration. This underscores the computational feasibility of the proposed methodology being more than 100 times faster than the computational speed available in established modelling frameworks such as our previously developed CEINMS toolbox. This fast computational time renders the model suitable for real-time exoskeleton control applications.

B. Control

When employing the predictive PD controller without constraints, maintaining the tendon force below the threshold posed significant challenges. Although the predictive PD without any constraints on the actuation of the actuator could keep the tendon force under the threshold, it required an actuation force of 8150 N (as depicted in Figure S-1-c supplementary material) to achieve this, which is impractical in reality. In the context of the constrained predictive PD controller, the controller encountered difficulties in keeping the tendon force below the designated threshold, especially when high muscle excitation amplitudes and elevated hopping frequencies coincided. As illustrated in Figure S-1-b, the constrained PD controller becomes active within similar time frames as the unconstrained version. However, the constrained version fell short of reaching the actuator limit in time to fully utilize the actuator's capacity. The observed discrepancy arises from the controller's reliance on errors from the following time instant despite having advanced knowledge of future MTU force through the output of the tendon force predictor and desired force estimator. This operational method contrasts with the NMPC controller's utilization of the entire control horizon. Furthermore, the behavior of the predictive PD controller varies significantly across different hopping excitation frequencies and amplitudes, with its performance heavily reliant on the tuning of the K_p and K_d gains. Therefore, better results might be achieved by designing an adaptive predictive PD controller.

The proposed NMPC-based approach offers significant advantages in controlling MTU force, e.g., Achilles tendon force. By accurately predicting future instances where the tendon force might exceed the permissible limit, the controller adjusts its actuation values preemptively. This approach successfully prevented the tendon force from surpassing the allowed threshold while maintaining it within a narrow range near the limit (median = 2993.7 N and STD = 57.3 N). As a result, the system provided improved control, enhanced stability, and greater user comfort. This effectiveness is further illustrated in Figure 5-b, which shows that during most periods of controller activity, the peak MTU force remained between 2950 N and 3000 N. Consequently, not only does it avoid instantaneous force generation, as observed in the unconstrained predictive PD, but also regulates the control effort over time to prevent increments from crossing the allowed threshold. Also, as depicted in Figure S-1-a, it is evident that the actuator force only approached the limit (without surpassing it) when the hopping excitation and frequency are high. This behavior can be attributed to the influence of the cost function, 8, on the actuator force (F^{ac}), wherein the actuator force directly impacts the energy consumption of the actuator. Furthermore, the findings indicated that the control outputs demonstrated nearly linear growth when $w_1 \gg w_2$ in the cost function. Increasing the weight w_2 would prompt the assistance profile to initiate earlier and increase more gradually.

As depicted in Figure 5-a, the worst-case scenario occurred when the muscle was highly excited and the hopping frequency was moderate or high. This observation is particularly intriguing and presents a potential avenue for further investigation in this study. It suggests that the natural frequency of the human plantarflexor system, in the absence of the exoskeleton, during hopping converges around this specific range. This finding aligns, to some extent, with the results of [39], which analyzed the frequencies of various animals and humans with different weights during walking and hopping. The discrepancy between the natural frequencies reported in this study and those in [39] may be attributed to the damping incorporated into the Hill-type muscle model used here. When examining this hypothesis, it is important to consider that the natural frequency can be influenced by the stiffness of the MTU [40]. As previously noted, the tendon stiffness in our model exhibits nonlinear behavior. During the simulation, the average stiffness of the Achilles tendon was approximately $420,000$ N/m. Furthermore, the average stiffness of the passive force element in the Hill-type muscle model was around $22,500$ N/m. Due to the pulley system, the effective loading of the weight must be accounted for by tripling its impact, resulting in an equivalent weight of 1.5 times the body weight per leg.

1) Sensitivity Analysis: Figure 7-a shows the performance of the controller in response to the uncertainty in the excitation. As shown, although the controller was not successful in keeping the tendon force under the prespecified threshold, it can keep it close to the threshold when the uncertainty was not higher than 10%. In other words, knowing the amplitude of the activation seems relevant. As depicted in Figure 7-a, when the excitation disturbance is positive (the controller is not aware of the increase in muscle excitation amplitude), the controller kept the tendon force below the threshold. This occurred because the controller anticipated surpassing the threshold sooner than reality, leading to premature engagement of the controller. Conversely, when the disturbance is negative, the controller maintains the tendon force at values exceeding the threshold. This discrepancy arised from the controller's misjudgment in detecting the surpassing of the threshold. Despite the actual threshold crossing, the controller perceived itself to be in the region below the threshold, thus failing to activate the actuator on time. To overcome this challenge, it is advantageous to predict the muscle excitation pattern within the control horizon.

When the subject's weight (or the center of pressure, CoP) changed without the controller's awareness, its behavior differed significantly from situations where the weight was accurately known. As shown in Figure 7-b, perceiving a higher weight for the subject caused the actuator to activate prematurely. This occurred because the controller, unaware of the subject's weight relief (or CoP change), assumed a larger acceleration due to the reduced weight. This led to a miscalculation, with the controller incorrectly predicting a rapid increase in tendon force.

On the other hand, when the subject's actual weight exceeded the weight assumed by the controller, the actuator's activation was delayed. This delay resulted from the tendon force predictor failing to identify the threshold crossing in time. However, in this case, the peak MTU force remained closer to the threshold because the NMPC received feedback from the system. Unlike open-loop controllers or predefined assistance profiles, the NMPC adjusted its output dynamically upon detecting that the tendon force had surpassed the threshold. This reactive adjustment did not occur in scenarios where the controller overestimated the subject's weight.

C. Limitations of Current Study and Future Works

The proposed predictive framework implemented tendon force feedback control within a low computational time of less than 14 *ms*, rendering it suitable for real-world applications. The MTU parameters, including maximum isometric force, optimal fiber length, and tendon slack length are personalized and obtained by a calibration phase, similar to the procedure that is done to calibrate the MTU model in CEINMS toolbox [26], [27]. In our analysis, we assumed pre-known muscle excitation/activation patterns. However, as demonstrated in the sensitivity analysis, the framework exhibited some sensitivity to muscle activation. To enhance the practical applicability of this control framework, a key strategy involves integrating a muscle activation predictor into the algorithm. An initial step towards this integration could be achieved by leveraging muscle synergies, as discussed in [30], [41]. However, muscular activation can be influenced by external perturbations, such as those from exosuit support, as well as changes in movement tasks. Therefore, a more robust approach would entail predicting muscular activation in the presence of exosuit assistance. The incorporation of a muscle activation predictor is expected to improve the framework's adaptability and resilience in real-world scenarios.

An additional notable finding from the sensitivity analysis conducted in the research paper was the framework's sensitivity to its estimation of user weight. While this sensitivity isn't a significant concern during controlled laboratory experiments due to the personalized models employed in the predictive control framework, it could pose challenges in real-world applications. One way to interpret the impact of changes in user weight is to view them as shifts in the COP concerning the controller's anticipated COP position, which is often near the metatarsal joint during late-stance or hopping activities. This interpretation underscores the importance of integrating the COP into the inner model of the NMPC algorithm before extending this work to more sophisticated cyclic motions such as walking and running.

As a future direction, the framework will be extended for real-time control of exoskeletons. This extension aims to bridge the gap between simulation-based validation and practical implementation, enabling the system to handle dynamic and unstructured environments using AI-based muscle activation or MTU force predictors. Real-time implementation will require addressing key challenges such as hardware constraints, computational efficiency, and robust sensor integration. Additionally, rather than estimating the current MTU length and load using the model (Fig. 2-a), these parameters will be directly acquired using sEMG and IMU sensors. This sensor-driven approach will enhance the accuracy and adaptability of the framework, making it more suitable for applications in assistive robotics and rehabilitation systems.

V. Conclusion

In conclusion, this paper introduces a framework for the closed-loop control of peak tendon force in a simulated human ankle joint system with parallel exoskeleton actuation. By employing NMPC in conjunction with a computationally efficient inner model governed by explicit, closed-form ODEs, we make a substantial stride in filling the existing gap in the control of biological tissue mechanics within the realm of robotic exoskeletons for controlling the peak tendon force.

Our approach integrates differentiable equations for a Hill-type MTU system with parallel damping and the equation of motion for a human leg with parallel exoskeleton actuation, encapsulated within the NMPC framework for the first time. The outcomes highlight the effectiveness of our proposed control framework, successfully maintaining tendon force below a predetermined threshold across diverse simulated conditions, including hopping with varying muscle excitation amplitudes and frequencies.

Looking ahead, the framework will be further developed for real-time application in exoskeleton control. The focus will be on addressing key challenges associated with real-time implementation, such as ensuring computational efficiency and enhancing adaptability to individual differences. These advancements will pave the way for broader adoption of the framework in clinical and industrial settings, enabling its application in assistive and rehabilitative technologies.

References

[1] M. Grimmer et al., "Comparison of the human-exosuit interaction using ankle moment and ankle positive power inspired walking assistance," *J. Biomech.*, vol. 83, pp. 76–84, Jan. 2019. [Online]. Available: https://www.sciencedirect.com/science/article/pii/S0021929018308583

[2] J. Zhang et al., "Human-in-the-loop optimization of exoskeleton assistance during walking," *Science*, vol. 356, no. 6344, pp. 1280—1284, Jun. 2017. [Online]. Available: https://doi.org/10.1126/science.aal5054

[3] K. A. Witte, P. Fiers, A. L. Sheets-Singer, and S. H. Collins, "Improving the energy economy of human running with powered and unpowered ankle exoskeleton assistance," *Sci. Robot.*, vol. 5, no. 40, pp. 1–8, 2020. [Online]. Available: https://api.semanticscholar.org/CorpusID:214671593

[4] Q. Chen, J. Wang, Q. Xiang, and S. Guo, "Bayesian algorithm-based force profiles optimization of hip-assistive soft exosuits under variable walking speeds," *IEEE Trans. Med. Robot. Bionics*, vol. 6, no. 3, pp. 1232–1244, Aug. 2024.

[5] P. S. Pridham and L. Stirling, "Ankle exoskeleton torque controllers based on soleus muscle models," *PLoS One*, vol. 18, no. 2, pp. 1–18, 2023. [Online]. Available: https://doi.org/10.1371/journal.pone.0281944

[6] S. Song and S. H. Collins, "Optimizing exoskeleton assistance for faster self-selected walking," *IEEE Trans. Neural Syst. Rehabil. Eng.*, vol. 29, pp. 786–795, 2021.

[7] K. A. Ingraham, C. D. Remy, and E. J. Rouse, "User preference of applied torque characteristics for bilateral powered ankle exoskeletons," in *Proc. IEEE RAS EMBS Int. Conf. Biomed. Robot. Biomechatronics*, 2020, pp. 839–845.

[8] G. S. Sawicki and D. P. Ferris, "Mechanics and energetics of level walking with powered ankle exoskeletons," *J. Exp. Biol.*, vol. 211, no. 9, pp. 1402–1413, May 2008.

[9] G. Durandau, W. F. Rampeltshammer, H. V. D. Kooij, and M. Sartori, "Neuromechanical model-based adaptive control of bilateral ankle exoskeletons: Biological joint torque and electromyogram reduction across walking conditions," *IEEE Trans. Robot.*, vol. 38, no. 3, pp. 1380–1394, Jun. 2022.

[10] D. D. Molinaro, K. L. Scherpereel, E. B. Schonhaut, G. Evangelopoulos, M. K. Shepherd, and A. J. Young, "Task-agnostic exoskeleton control via biological joint moment estimation," *Nature*, vol. 635, no. 8038, pp. 337–344, 2024. [Online]. Available: https://doi.org/10.1038/s41586-024-08157-7

[11] S. L. McNamara et al., "Anti-inflammatory therapy enables robot-actuated regeneration of aged muscle," *Sci. Robot.*, vol. 8, no. 76, 2023, Art. no. eadd9369. [Online]. Available: https://www.science.org/doi/abs/10.1126/scirobotics.add9369

[12] D. G. Schmitz et al., "Modulation of Achilles tendon force with load carriage and exosuit assistance," *Sci. Robot.*, vol. 7, no. 71, Oct. 2022, Art. no. eabq1514. [Online]. Available: https://www.science.org/doi/abs/10.1126/scirobotics.abq1514 https://www.science.org/doi/10.1126/scirobotics.abq1514 http://www.ncbi.nlm.nih.gov/pubmed/36260697

[13] P. Slade, M. J. Kochenderfer, S. L. Delp, and S. H. Collins, "Personalizing exoskeleton assistance while walking in the real world," *Nature*, vol. 610, no. 7931, pp. 277–282, Oct. 2022. [Online]. Available: https://www.nature.com/articles/s41586-022-05191-1

[14] X. Bao, V. Molazadeh, A. Dodson, B. E. Dicianno, and N. Sharma, "Using person-specific muscle fatigue characteristics to optimally allocate control in a hybrid exoskeleton—preliminary results," *IEEE Trans. Med. Robot. Bionics*, vol. 2, no. 2, pp. 226–235, Mar. 2020.

[15] C. Caulcrick, W. Huo, E. Franco, S. Mohammed, W. Hoult, and R. Vaidyanathan, "Model predictive control for human-centred lower limb robotic assistance," *IEEE Trans. Med. Robot. Bionics*, vol. 3, no. 4, pp. 980–991, Nov. 2021.

[16] A. F. Huxley and R. Niedergerke, "Structural changes in muscle during contraction: Interference microscopy of living muscle fibres," *Nature*, vol. 173, no. 4412, pp. 971–973, 1954. [Online]. Available: https://doi.org/10.1038/173971a0

[17] H. Huxley and J. Hanson, "Changes in the cross-striations of muscle during contraction and stretch and their structural interpretation," *Nature*, vol. 173, no. 4412, pp. 973–976, 1954. [Online]. Available: https://doi.org/10.1038/173973a0

[18] A. H. Caillet, A. T. M. Phillips, C. Carty, D. Farina, and L. Modenese, "Hill-type computational models of muscle-tendon actuators: A systematic review," bioRxiv, 2022. [Online]. Available: https://www.biorxiv.org/content/early/2022/11/24/2022.10.14.512218

[19] M. Sartori, M. Reggiani, A. J. van den Bogert, and D. G. Lloyd, "Estimation of musculotendon kinematics in large musculoskeletal models using multidimensional B-splines," *J. Biomech.*, vol. 45, no. 3, pp. 595–601, 2012. [Online]. Available: https://www.sciencedirect.com/science/article/pii/S0021929011006828

[20] C. Anderson, "Equations for modeling the forces generated by muscles and tendons," presented at Physics-Based Simulat. Biol. Struct., 2007.

[21] A. van den Bogert, D. Blana, and D. Heinrich, "Implicit methods for efficient musculoskeletal simulation and optimal control," *Procedia IUTAM*, vol. 2, pp. 297–316, May2011.

[22] F. De Groote, A. Kinney, A. Rao, and B. Fregly, "Evaluation of direct collocation optimal control problem formulations for solving the muscle redundancy problem," *Ann. Biomed. Eng.*, vol. 44, pp. 2922–2936, Mar. 2016.

[23] M. Millard, T. Uchida, A. Seth, and S. L. Delp, "Flexing computational muscle: Modeling and simulation of musculotendon dynamics," *J. Biomech. Eng.*, vol. 135, no. 2, pp. 210051Ű-2100511, Feb. 2013. [Online]. Available: https://doi.org/10.1115/1.4023390

[24] M. Nabipour, G. S. Sawicki, and M. Sartori, "Predictive control of peak Achilles tendon force in a simulated system of the human ankle joint with a parallel artificial actuator during hopping," in *Proc. Int. Conf. Rehabil. Robot. (ICORR)*, Sep. 2023, pp. 1–6. [Online]. Available: http://www.ncbi.nlm.nih.gov/pubmed/37941182 https://ieeexplore.ieee.org/document/10304771/
[25] M. Nabipour and M. Sartori, "Closed-form modeling of the soleus musculotendon unit," in *Proc. 28th Congr. Eur. Soc. Biomech.*, 2023, p. 1.
[26] C. Pizzolato et al., "CEINMS: A toolbox to investigate the influence of different neural control solutions on the prediction of muscle excitation and joint moments during dynamic motor tasks," *J. Biomech.*, vol. 48, no. 14, pp. 3929–3936, 2015. [Online]. Available: https://www.sciencedirect.com/science/article/pii/S0021929015005151
[27] M. Sartori et al., "CEINMS-RT: An open-source framework for the continuous neuro-mechanical model-based control of wearable robots," TechRxiv, 2025. [Online]. Available: https://www.techrxiv.org/
[28] M. Nabipour, G. S. Sawicki, and M. Sartori, "Predictive control for bio-protective robotic exoskeletons: Closed-loop control of internal body forces," Zenodo, Sep. 2024. [Online]. Available: https://doi.org/10.5281/zenodo.13828172
[29] M. Nabipour, G. S. Sawicki, and M. Sartori, "Predictive closed-loop control of musculotendon force: Towards a framework for human locomotion," in *Proc. 10th IEEE RAS/EMBS Int. Conf. Biomed. Robot. Biomechatronics (BioRob)*, 2024, pp. 1778–1783.
[30] Y. Li, M. Sartori, and M. Nabipour, "Towards predictive control of trunk internal loads: modeling musculotendon loads and predicting muscle excitations," in *Converging Clinical and Engineering Research on Neurorehabilitation V*, J. L. Pons, J. Tornero, and M. Akay, Eds. Cham, Switzerland: Springer Nat., 2025, pp. 164–168.
[31] D. G. Thelen, "Adjustment of muscle mechanics model parameters to simulate dynamic contractions in older adults," *J. Biomech. Eng.*, vol. 125, no. 1, pp. 70–77, 2003.
[32] B. D. Robertson, D. J. Farris, and G. S. Sawicki, "More is not always better: Modeling the effects of elastic exoskeleton compliance on underlying ankle muscle–tendon dynamics," *Bioinspir. Biom.*, vol. 9, no. 4, Nov. 2014, Art. no. 46018. [Online]. Available: https://dx.doi.org/10.1088/1748-3182/9/4/046018
[33] B. D. Robertson and G. S. Sawicki, "Exploiting elasticity: Modeling the influence of neural control on mechanics and energetics of ankle muscle-tendons during human hopping," *J. Theor. Biol.*, vol. 353, pp. 121–132, Jul. 2014.
[34] L. Wang, E. H. F. van Asseldonk, and H. van der Kooij, "Model predictive control-based gait pattern generation for wearable exoskeletons," in *Proc. IEEE Int. Conf. Rehabil. Robot.*, 2011, pp. 1–6.
[35] M. Nabipour, G. S. Sawicki, and M. Sartori, "Predictive control of musculotendon loads across fast and slow-twitch muscles in a simulated system with parallel actuation," *Wearable Technol.*, vol. 6, p. e8, Feb. 2025.
[36] C. P. Cop, G. Durandau, A. M. Esteban, R. C. van 't Veld, A. C. Schouten, and M. Sartori, "Model-based estimation of ankle joint stiffness during dynamic tasks: A validation-based approach," in *Proc. 41st Annu. Int. Conf. IEEE Eng. Med. Biol. Soc. (EMBC)*, 2019, pp. 4104–4107.
[37] H. Wang, A. Basu, G. Durandau, and M. Sartori, "Comprehensive kinetic and EMG dataset of daily locomotion with 6 types of sensors," Biomech. Eng., Univ. Twente, Enschede, The Netherlands, 2022. [Online]. Available: https://doi.org/10.5281/zenodo.6457662
[38] G. Durandau, D. Farina, and M. Sartori, "Robust real-time musculoskeletal modeling driven by Electromyograms" *IEEE Trans. Biomed. Eng.*, vol. 65, no. 3, pp. 556–564, Mar. 2018.
[39] G. A. Cavagna and M. A. Legramandi, "Running, hopping and trotting: Tuning step frequency to the resonant frequency of the bouncing system favors larger animals." *J. Exp. Biol.*, vol. 218, no. Pt20, pp. 3276–3283, Oct. 2015.
[40] G. A. Cavagna, M. Mantovani, P. A. Willems, and G. Musch, "The resonant step frequency in human running" *Pflugers Archiv. Eur. J. Physiol.*, vol. 434, no. 6, pp. 678–684, Nov. 1997.
[41] J. Gonzalez-Vargas, M. Sartori, S. Dosen, D. Torricelli, J. Pons, and D. Farina, "A predictive model of muscle excitations based on muscle modularity for a large repertoire of human locomotion conditions," *Front. Comput. Neurosci.*, vol. 9, p. 114, Sep. 2015. [Online]. Available: https://www.frontiersin.org/articles/10.3389/fncom.2015.00114